HHS Public Access

Author manuscript

Nat Genet. Author manuscript; available in PMC 2018 August 14.

Published in final edited form as:

Nat Genet. 2015 September ; 47(9): 1056–1060. doi:10.1038/ng.3370.

Genomic analysis of mycosis fungoides and Sézary syndrome identifies recurrent alterations in TNFR2

Alexander Ungewickell[1,2,12], **Aparna Bhaduri**[1,12], **Eon Rios**[1], **Jason Reuter**[3], **Carolyn S Lee**[1], **Angela Mah**[1], **Ashley Zehnder**[1], **Robert Ohgami**[4], **Shashikant Kulkarni**[5,6,7], **Randall Armstrong**[8], **Wen-Kai Weng**[8], **Dita Gratzinger**[4], **Mahkam Tavallaee**[9], **Alain Rook**[10], **Michael Snyder**[3], **Youn Kim**[9], and **Paul A Khavari**[1,11]

[1]Program in Epithelial Biology, Stanford University, Stanford, California, USA.

[2]Division of Hematology, Stanford University, Stanford, California, USA.

[3]Department of Genetics, Stanford University, Stanford, California, USA.

[4]Department of Pathology, Stanford University, Stanford, California, USA.

[5]Department of Pathology and Immunology, Washington University School of Medicine, St. Louis, Missouri, USA.

[6]Department of Pediatrics, Washington University School of Medicine, St. Louis, Missouri, USA.

[7]Department of Genetics, Washington University School of Medicine, St. Louis, Missouri, USA.

[8]Division of Blood and Marrow Transplantation, Stanford University, Stanford, California, USA.

[9]Multidisciplinary Cutaneous Lymphoma Program, Stanford University, Stanford, California, USA.

[10]Department of Dermatology, Perelman School of Medicine, University of Pennsylvania, Philadelphia, Pennsylvania, USA.

[11]Veterans Affairs Palo Alto Healthcare System, Palo Alto, California, USA.

[12]These authors contributed equally to this work.

Abstract

Mycosis fungoides and Sézary syndrome comprise the majority of cutaneous T cell lymphomas (CTCLs), disorders notable for their clinical heterogeneity that can present in skin or peripheral blood. Effective treatment options for CTCL are limited, and the genetic basis of these T cell

Correspondence should be addressed to P.A.K. (khavari@stanford.edu).

AUTHOR CONTRIBUTIONS

A.U. and A.B. designed and executed experiments, analyzed data and wrote the manuscript. E.R., C.S.L., J.R., A.M., A.Z., R.O., S.K., R.A., W.-K.W. and D.G. helped execute experiments, analyzed data and contributed to the design of experimentation. M.T. performed clinical data analysis. M.S. helped design experiments. A.R. and Y.K. provided clinical data and analysis. P.A.K. designed experiments, analyzed data and wrote the manuscript.

Accession codes. Sequencing data have been deposited in the database of Genotypes and Phenotypes (dbGaP) under accession phs000913.v1.p1.

Note: Any Supplementary Information and Source Data files are available in the online version of the paper.

COMPETING FINANCIAL INTERESTS

The authors declare no competing financial interests.

lymphomas remains incompletely characterized[1]. Here we report recurrent point mutations and genomic gains of *TNFRSF1B*, encoding the tumor necrosis factor receptor TNFR2, in 18% of patients with mycosis fungoides and Sézary syndrome. Expression of the recurrent TNFR2 Thr377Ile mutant in T cells leads to enhanced non-canonical NF-ºB signaling that is sensitive to the proteasome inhibitor bortezomib. Using an integrative genomic approach, we additionally discovered a recurrent *CTLA4-CD28* fusion, as well as mutations in downstream signaling mediators of these receptors.

We performed whole-exome sequencing on 11 mycosis fungoides and Sézary syndrome samples each paired with a normal sample to identify somatic genetic alterations associated with these malignancies (Supplementary Table 1). A total of 494 genes were selected for deep targeted resequencing, which included genes mutated in the exome data set, genes previously implicated in the pathogenesis of T cell malignancies and related pathway members (Supplementary Tables 2–7). A total of 91 individual samples and cell lines were sequenced at an average coverage of ~700×, of which 73 were included in our mycosis fungoides and Sézary syndrome paired analysis with normal samples (Supplementary Fig. 1 and Supplementary Table 8). The mutational spectrum of mycosis fungoides and Sézary syndrome is heterogeneous, with the tumor-suppressor genes *MLL3* (also known as *KMT2C*; 26%) and *TP53* (13%) being the two most frequently mutated genes (Supplementary Fig. 2). Furthermore, we found gain-of-function mutations in *KRAS* and *PLCG1* that have previously been reported in mycosis fungoides and Sézary syndrome[2,3]. The most frequent recurrent point mutation in our data set occurred at codon 377 of *TNFRSF1B* (5%; 4/73), encoding tumor necrosis factor receptor 2 (TNFR2), resulting in a recurrent TNFR2 Thr377Ile mutant. TNFR2 is a receptor that regulates key T cell signaling pathways and has not previously been implicated in cancer (Fig. 1a)[4].

We noted that many somatic alterations involved pathways related to TNFR2 and non-canonical nuclear factor (NF)-ºB signaling, primarily regulating T cell survival and proliferation (Fig. 1a), including the TNFR2 pathway itself, as well as the T cell receptor (TCR) and CD28 pathways. This finding is consistent with previous transcriptome sequencing indicating differential expression of genes in the TCR signaling pathway between Sézary syndrome cells and autologous polyclonal $CD4^+$ T cells[5]. In addition to alterations in TNFR2, we found mutations in phosphoinositide 3-kinase (PI3K)-related genes involved in TCR-CD28 signaling and mutations in NF-ºB pathway genes, including a subset in the canonical NF-ºB signaling pathway (Supplementary Fig. 2b), that control transcriptional programs downstream of key T cell signaling pathways (Fig. 1a,b)[4].

Structural variations frequently characterize malignancies of lymphoid origin, and we therefore used FACTERA to detect chromosomal structural variations in mycosis fungoides and Sézary syndrome samples[6]. This analysis identified structural variation events (excluding copy number gains) in pathways related to T cell survival and proliferation in 11% of patients with mycosis fungoides or Sézary syndrome (Supplementary Table 9). Interestingly, the structural variants were largely mutually exclusive with the TNFR2 alterations (Fisher's exact test, $P = 0.0005$). The structural variants included *NFKB2* gene truncations in 5% (4/73) of cases with the deletion of a region whose loss is known to

generate a truncated p100 protein with predicted proteasome-independent NF-ºB2 nuclear localization[7,8] (Fig. 2a), as well as a deletion involving *TRAF3* that would also be expected to increase non-canonical NF-ºB signaling (Fig. 2b). We also identified a translocation altering the *TP63* gene recently reported to be rearranged in T cell lymphomas (Supplementary Fig. 3a,b)[9], two translocations predicted to disrupt the *CD274* gene, encoding PD-L1, which normally inhibits T cell activation via PD1 binding (Fig. 2c)[10], and a translocation predicted to delete the pro-apoptotic *TNFRSF10A* receptor (Supplementary Fig. 3c,d)[11].

We further detected in two patients a large deletion on chromosome 2 involving the functionally antagonistic surface receptors CTLA4 and CD28, fusing the extracellular portion of the inhibitory CTLA4 protein to the co-activating cytoplasmic tail of CD28 (Fig. 2d and Supplementary Fig. 3e–g). CTLA4 binds the shared ligands (B7-1 and B7-2) with higher affinity and avidity than CD28, and, on the basis of experiments in mouse T cells, an extracellular CTLA4 domain fused to the signaling domain of CD28 would be expected to transmit powerful co-stimulatory signals in T cells[12]. Consistent with this expectation, Jurkat cells engineered to express this fusion construct proliferated faster than cells with empty vector or those overexpressing CTLA4 (Fig. 2e and Supplementary Fig. 3h). Consequently, the CTLA4-CD28 fusion may be an oncogenic driver in a subset of patients with mycosis fungoides and Sézary syndrome that leads to enhanced lymphoma cell proliferation in a normally inhibitory cellular milieu. This fusion may represent a therapeutic opportunity in this subset of patients for use of the CTLA4-blocking antibody ipilimumab[13], a possibility supported by a recent study of a single case[14].

TNFR2 expression is restricted to a few cell types, including mature T cells, where it enhances T cell activation and survival via non-canonical NF-κB signaling[15]. Interestingly, patients with mycosis fungoides or Sézary syndrome frequently also have genomic gains of a 1.25-Mb region of chromosome 1p36.2 that includes the *TNFRSF1B* (TNFR2) locus[16], and in peripheral T cell lymphomas higher levels of soluble TNFR2 are prognostic for poor outcome[17]. We used digital droplet PCR (ddPCR) to confirm that the *TNFRSF1B* (TNFR2) locus was subject to somatically acquired copy number gain in 14% (10/73) of patients with mycosis fungoides and Sézary syndrome in our cohort and also demonstrated this gain in one additional patient by FISH analysis (Figs. 1b and 3a,b, and Supplementary Fig. 4a). This gain correlated with increased *TNFRSF1B* transcript levels in patient tumor samples and with increased TNFR2 protein levels in the HH CTCL cell line that harbors this gain[18] (Fig. 3c–e and Supplementary Fig. 4b). In total, *TNFRSF1B* was altered in 18% (13/73) of patients with mycosis fungoides and Sézary syndrome by either point mutation or gain, suggesting a potential role of oncogenic TNFR2 signaling in the development of these diseases.

In the context of a heterogeneous mutation landscape, 38% (28/73) of the patients sequenced demonstrated a genetic abnormality in TNFR2-related T cell signaling pathways. *TNFRSF1B* lesions were the only alterations that were statistically enriched in Sézary syndrome in comparison to mycosis fungoides ($P = 0.0043$; Supplementary Table 10). The distribution of *TNFRSF1B* lesions was significantly enriched in stage IV disease ($P = 0.0073$). Moreover, patients with mycosis fungoides and lesions in the TNFR2-related

pathway were significantly enriched for large-cell transformation (LCT; $P = 0.007$), which correlated with a higher overall mutation rate and poorer survival in our cohort (Supplementary Fig. 5a,b). Multivariate analysis suggested that, although TNFR2 pathway mutations are statistically correlated with worse survival, these findings are confounded by stage and LCT status, which are independent predictors of survival (Supplementary Fig. 5b–d and Supplementary Table 11). Of note, several other parameters examined did not correlate with differences in patient survival, including number of mutations, age, diagnosis or other mutation combinations (Supplementary Fig. 5e–i).

Analysis of previous Sézary syndrome transcriptome data[5] identified increased *TNFRSF1B* transcript levels in Sézary syndrome in all three patients analyzed in comparison with autologous polyclonal $CD4^+$ T cells (Fig. 3f). Using gene set enrichment analysis (GSEA), we identified the TNF pathway as the highest-scoring TNFR2-dependent expression signature in 24 patients with mycosis fungoides (Fig. 4a). This result suggested that alterations in TNFR2 levels in this context meaningfully alter TNF pathway signaling to affect gene expression in this lymphoma.

The observed recurrent *TNFRSF1B* c. 1130C>T mutation resulting in p.Thr377Ile involves a highly conserved threonine residue in the TRAF2 regulatory domain of TNFR2 (Fig. 4b,c)[19]. To test the potential functional impact of this substitution, we introduced either the wild-type or mutant receptor at physiological expression levels into Jurkat cells that do not express endogenous TNFR2 and assessed non-canonical NF-κB pathway activation (Supplementary Fig. 6a,b). Specifically, we analyzed TRAF2 levels and processing of p100 to p52 by immunoblotting. We found that TNFR2 Thr377Ile expression led to increased TRAF2 degradation and proteolytic processing of p100 to p52 in comparison to expression of wild-type TNFR2 (Fig. 4d–f). In a subcutaneous tumor model in mice, tumors expressing wild-type TNFR2 or TNFR2 Thr377Ile grew to larger size than tumors with an empty vector control (Supplementary Fig. 7a).

As expected, the Jurkat cells expressing wild-type TNFR2 and TNFR2 Thr377Ile underwent alterations in gene expression that involved the TNFR2 signature identified in patients with mycosis fungoides (Fig. 4g,h). Consistent with the enhanced proteolytic processing of the *NFKB2* gene product p100, we determined that the amplitude of NF-κB target gene expression was significantly increased by expression of TNFR2 Thr377Ile in comparison to wild-type TNFR2 (Fig. 4i). Previous studies showing increased NF-κB activity in patients with CTCL motivated early-phase clinical studies of the proteasome inhibitor bortezomib in this disease[20]. On the basis of the observed therapeutic benefit in a subset of patients, we treated Jurkat cells expressing wild-type or mutant TNFR2 with bortezomib, leading to a reversal in the expression of a subset of the TNFR2-responsive genes that were statistically enriched for leukocyte activation, signaling and apoptosis (Fig. 4j). Interestingly, the Jurkat cells expressing wild-type TNFR2 or TNFR2 Thr377Ile were more responsive to bortezomib than control cells with empty vector, suggesting that TNFR2 pathway activation is specifically targeted by this proteasome inhibitor (Supplementary Fig. 7b). To further test this hypothesis, we used HH cells, a CTCL cell line that contains a *TNFRSF1B* (TNFR2) genomic gain[18], and CRISPR-Cas9 technology to generate an HH TNFR2-knockout line (Supplementary Fig. 7c). As predicted, the TNFR2-knockout HH cells were less sensitive to

bortezomib treatment, despite no significant differences in cell viability under normal growth conditions (Supplementary Fig. 7d,e). Additionally, we compared HH cells to Hut78 cells that contain an *NFKB2* gene truncation[8]; as expected, the Hut78 cells were less sensitive to the proteasome inhibitor than HH cells (Supplementary Fig. 7f). These data provide a mechanistic rationale for the activity of bortezomib observed in a subpopulation of patients with mycosis fungoides and Sézary syndrome and warrant further testing of TNFR2 pathway alterations as a predictive biomarker for the efficacy of proteasome inhibitor therapy in this disease.

In this study, we identify recurrent alterations in the TNFR2 pathway in addition to other genes regulating T cell survival and proliferation that affect more than a third of patients with mycosis fungoides and Sézary syndrome. Of these patients, over half may benefit from either approved medications or drugs currently in clinical development targeting PI3K isoforms, CTLA4 and NF-κB processing. Future studies are needed to investigate the efficacy of targeted agents in patients with mycosis fungoides and Sézary syndrome prospectively selected on the basis of their genomic profiles.

METHODS

Methods and any associated references are available in the online version of the paper.

ONLINE METHODS

Cutaneous T cell lymphoma samples.

CTCL and matched normal control samples were collected with informed consent prospectively under a protocol approved by the Institutional Review Board at Stanford University Medical Center (IRB21750). Skin biopsies were stored in RNAlater (Ambion), and peripheral blood samples were processed by Ficoll gradient centrifugation, magnetic bead–mediated CD4 selection (Miltenyi) or flow cytometry to separate lymphoma cells from other peripheral blood leukocytes. Primarily skin biopsies were used for patients with a mycosis fungoides diagnosis and sorted or enriched lymphoma cells were used for patients with Sézary syndrome, although there were a few exceptions (Supplementary Table 9). All patient characteristics used for genomic analysis are from the time of biopsy, except for the patient's original diagnosis of either mycosis fungoides or Sézary syndrome.

Cell culture

Jurkat cells, HH cells and Hut78 cells were obtained from the American Type Culture Collection (ATCC); MyLa and SeAx cells were a generous gift from K. Kalthoft (Aarhus University). Cells were grown in RPMI-1640 medium (Life Technologies) supplemented with 10% BCS (Jurkat, HH and MyLa cells), IMDM supplemented with 20% BCS (Life Technologies) (Hut78 cells) or primary T cell medium (SeAx cells; RPMI-1640 medium supplemented with 14 μM β-mercaptoethanol, 10% BCS, 5% human AB serum (Sigma), 200 IU/ml interleukin (IL)-2, 20 ng/ml IL-7 and 20 ng/ml IL-15 (Peprotech)). All cells were grown at 37 °C in a humidified chamber with 5% CO_2 and were routinely tested for mycoplasma contamination.

Library preparation and sequencing.

Exome sequencing libraries were prepared using the TruSeq DNA Library Prep kit, and enrichment was performed with EZexome V2.0 Early Access for Capture by Ambry Genetics. Genes for targeted resequencing were chosen on the basis of mutation in the original whole-exome sequencing data together with additional targets related to genes that were mutated and genes previously reported to be mutated in T cell lymphomas. Targeted resequencing libraries were prepared using the Illumina TruSeq kit (starting with 1 μg of genomic DNA) with barcodes. Libraries were pooled, and capture was performed with two distinct capture reagents targeting 1.2-Mb and 3.1-Mb regions of interest (SeqCap EZ, NimbleGen, Roche). The SeqCap EZ custom capture reagent is a solution-based capture protocol that uses specific regions of interest from pre-prepared libraries to enable targeted capture followed by resequencing. Before library preparation, certain DNA samples without sufficient amounts of starting material underwent whole-genome amplification (GenomePlex, Sigma). The libraries were sequenced with the Illumina HiSeq platform using 101-bp paired-end sequencing. RNA sequencing libraries were generated with the Illumina RNA TruSeq kit. Libraries were barcoded, pooled and sequenced with the Illumina HiSeq platform using 101-bp paired-end sequencing.

SNP arrays.

SNP array analysis was performed on the HH, Hut78, MyLa and SeAx cell lines as well as Sézary syndrome 15 DNA using the Affymetrix SNP 6.0 chip. SNP calls were made using the Affymetrix Genotyping Console 4.0. Using the set of SNPs that were identified as differing from the hg19 reference genome for all of the SNP arrays that also fell into the resequencing capture regions, sensitivity was calculated as the fraction of these SNPs that were identified as differing from the reference and specificity was calculated as the fraction of these SNPs that were identified to have the same genotype.

Single-nucleotide variant and fusion analysis.

Paired-end alignment was performed with Burrows-Wheeler Aligner (BWA)[22] to the hg19 reference using default parameters. Single-nucleotide variant (SNV) calling was performed by the Genome Analysis Toolkit (GATK)[23], VarScan[24] and SeqGene[25]. GATK was run by following the Best Practices v3 guidelines for exomes, using Indel Realignment, the Unified Genotyper, the Variant Quality Score Recalibrator and Variant Filtration as recommended[23]. Quality scores of ≥50 were required for a call, whereas a quality score of ≥10 was accepted for emitting. Recalibration was performed to the 1000 Genomes Project and HapMap 3.3 SNPs provided in the resource bundle. Resequencing analysis was recalibrated to the Mills and 1000 Genomes Gold Standard package with a maximum Gaussians parameter of 4. Variants were further filtered for clusters of greater than three SNVs in a 10-bp window. VarScan was run with default parameters. SeqGene was run with a threshold of 0.1 for SNV calling, and all other parameters were default. No minimum threshold was set for the resequencing analysis. Exome sequencing downstream analysis of GATK-called SNVs was performed on calls in a tranche of 99.0 or better. VarScan and SeqGene results were further filtered for false positives by removing any calls not supported by at least one read in each direction in the exome sequencing analysis. Unequal forward and reverse read distributions

(beyond an 80%/20% split) were also removed from analysis. Low-coverage calls (<6 reads) were not held to this standard, but rather variant calls had to comprise at least 20% of the reads at that position. Resequencing was performed in two batches. Resequencing downstream analysis was performed on all acquired mutation calls on the basis of the genotype designated by the SNV caller. It was further required that the CTCL samples contain ≥2-fold enrichment of reads supporting the mutation in comparison to the control samples. For cell lines and patients with CTCL without a matched normal control sample, a minimum variant allele frequency of 0.1 was required. Annotations for all mutation calls were performed with SeattleSeq[26]. For patient samples that underwent whole-genome amplification, we found that amplification introduced many mutations. To avoid studying false positive mutations, all mutations that involved samples undergoing whole-genome amplification were excluded from analysis, figures and tables (but are included as a reference in dbGaP). Patient samples that did not have matched control samples were also not considered in further analyses but are included in the supplementary tables. Fusion analysis was performed with FACTERA using default parameters on aligned BAM files from resequencing. Fusion validation was performed using genomic PCR; the resulting products were gel purified from a 1% agarose gel and sequenced by Sanger sequencing (Elim Biopharmaceuticals). Statistics to evaluate the enrichment of *TNFRSF1B* mutations in stage IV disease were calculated using Fisher's exact test.

Selection of patients for various analyses.

Our core analysis was based on the 73 patients with matched pairs, including the sample from patient mycosis fungoides 46 that underwent whole-genome amplification but whose TNFR2 p.Thr377Ile alteration was confirmed in the DNA before the amplification step. A total of 41 patients with mycosis fungoides and 32 patients with Sézary syndrome were analyzed in this study. All other mutations from mycosis fungoides 46 that were not validated by Sanger sequencing were excluded to avoid presenting false positive mutations. The characteristics for the 73 patients are described in Supplementary Table 9. Of note, only 61 of the 73 patients contained mutations in our panel of resequencing genes; the mutations for these 61 patients are included in Supplementary Table 2. The 14 patients without matched control samples and those that underwent whole-genome amplification, as well as 4 CTCL cell lines (HH, Hut78, MyLa and SeAx cells), were not considered in further analyses as mutations could not be determined to be somatically acquired. We also sequenced the Jurkat cell line (a T cell leukemia line) and H9 cells (a subclone of Hut78 cells) that were not counted in our total of 91 samples as they are not unique CTCL samples. We included the mutations (from unmatched patient samples and cell lines) and source sequencing files on dbGaP (for unmatched patient samples, cell lines and whole genome–amplified samples) that were not considered in our analysis denominators to allow future researchers the opportunity to check for specific mutation(s) of interest.

Digital droplet PCR.

Genomic gains of *TNFRSF1B* were identified using ddPCR. ddPCR experiments were performed according to the manufacturer's guidelines (Digital Droplet PCR Application Guide, Bulletin 6407 Rev A) on a Bio-Rad QX100 system. Briefly, 50–200 ng of genomic DNA was digested with HindIII at 37 °C for 1 h. ddPCR assays were performed using 20 ng

of digested genomic DNA, ddPCR supermix (Bio-Rad, 290-10420) and TaqMan probes against *TNFRSF1B* (FAM dye–labeled test probe) and *RPP30* (VIC dye–labeled diploid reference probe; ABI, 4403326). We subjected 20-μ1 reactions to the following cycling program: 10 min at 95 °C, 40 cycles of 30 s at 95 °C and 1 min at 60 °C, and 10 min at 98 °C. Sample quantification was performed using QuantaSoft version 1.3.2. A cohort of 89 primary tumors and cell lines was initially screened in duplicate for copy number gains at the *TNFRSF1B* locus. Sample Sézary syndrome 120 was the only sample that was too dilute to interpret the results. Samples exceeding a *TNFRSF1B* gene ratio of 2.15 in tumor versus normal cells, which corresponds to 15% of the cell population exhibiting a 3*N* state, were reanalyzed with triplicate measurements and compared to measurements on paired normal samples where possible. Statistical analysis was performed using a two-sided *t* test, and samples with $P < 0.05$ were considered to contain a *TNFRSF1B* gain.

Conservation analysis.

Conservation analysis was performed with a composite scoring metric from dbNSFP. dbNSFP (2.0)[27] was used to calculate the deleteriousness of mutating codons across *TNFRSF1B*. The scores from SIFT, PolyPhen HDIV, PolyPhen HDAV, LRT Prediction and MutationTaster were scaled from 0 to 1, with 1 being the most deleterious. These scores were summed and averaged if necessary for a given codon, resulting in a composite score that was represented on a heat map with darker red indicating a more deleterious outcome of mutation at that codon.

RNA sequencing analysis.

Paired-end alignment was performed using TopHat2 with default parameters[28]. Differential expression was called using CuffDiff2 default parameters and quantile normalization. GSEA[29] was run using *TNFRSF1B* expression levels as the phenotype, with 1,000 permutations and phenotypic permutation types. Classic Pearson analysis was used for scoring. Statistics for differences in fold change were performed using a Student's *t* test.

Lentiviral gene transfer.

All lentiviral gene transfection was performed by transfecting plasmids of interest into HEK293T cells obtained from the American Type Culture Collection (ATCC; ATCC verified and tested for mycoplasma) with helper plasmids, and virus was collected at 48 and 72 h. Virus was concentrated 40-fold using LentiX Concentrator (Clontech), and viral infection was performed in the presence of 1 μg/ml polybrene.

Immunoblotting.

Cells were lysed in modified RIPA buffer (50 mM Tris, pH 7.3, 0.5% sodium deoxycholate, 1% NP-40, 0.01% SDS and 150 mM NaCl) supplemented with EDTA-free protease inhibitor cocktail tablets. Cells were sonicated, and lysates were analyzed by immunoblotting. Immunoblot quantification was performed using ImageStudioLite software. The primary antibodies used were from Cell Signaling Technology, including antibodies to TNFR2 (rabbit, 3727), TRAF2 (rabbit, 4724) and NF-κB2 (rabbit, 3017S), and Sigma-Aldrich, including antibody to tubulin (mouse, T5326). Representative original

immunoblots are included (Supplementary Fig. 8), and statistics were performed using a Student's *t* test.

Flow cytometry.

Cells were washed in PBS with 1% FBS and incubated on ice with the indicated antibodies to human protein (TNFR2-APC (R&D Systems, FAB226A) or CTLA4-biotin (BD Pharmingen, 555852)) or isotype control (BD Pharmingen, 560720). Cells were then washed in PBS with 1% FBS, and those stained with antibody to CTLA4 were further stained on ice with streptavidin-APC molecules. Cells were resuspended in PBS with 1% FBS and propidium iodide and interrogated on a BD FACSCalibur instrument. The data were analyzed and processed using Flowjo software (Treestar).

Subcutaneous tumor experiment.

Subcutaneous tumors were generated by injecting 5 million Jurkat cells transduced with empty vector or expressing either wild-type or mutant TNFR2 into the right flank of 6-week-old nude mice (Jackson Laboratory, 005557). Experiments were performed under a protocol reviewed by the Stanford University Administrative Panel on Laboratory Animal Care (APLAC), protocol number 9863, and were compliant with standard ethical regulations. Mice were weighed and palpated for tumors at least once weekly. Once tumors were large enough to measure, calipers were used by A.B. and A.Z. to independently measure the tumors in three dimensions; these measurements were averaged and used to calculate spherical tumor volumes. A total of ten mice were used per group and were randomly assigned to groups on the basis of the cage they were in when delivered; no mice were excluded from any analyses. NCBI guidelines were consulted for this sample size, taking into consideration Type I error $\alpha = 0.05$ and power to detect change $\beta = 0.8$. The experiment was first carried out with 5 mice per group (15 mice; investigators were blinded to the identities of the groups) and then repeated to confirm the results from the first experiment. ANOVA statistical analyses were performed to identify differences between the groups.

Cell viability assays.

Cell viability assays to measure dose response to drug or cell proliferation were conducted using CellTiterBlue (CTB) reagent (Promega). CTB reagent was used at a 5× concentration and incubated with 200 μl of cells and medium for 2 h at 37 °C. Viability was analyzed using a SpectraMax M5 plate reader with excitation at 560 nm and emission at 590 nm.

CRISPR-Cas9 knockout.

CRISPR-Cas9 technology was used to knock out *TNFRSF1B* with the principles described previously[30]. *TNFRSF1B* guide RNA or a control guide RNA (Supplementary Table 12) was cloned into the lentiC-RISPRv2 plasmid (Addgene, 52961). After viral infection and 1 week of puromycin selection, HH cells were sorted using flow cytometry to isolate a TNFR2-null population. This population was expanded and used for experiments.

FISH analysis.

Interphase FISH was performed on formalin-fixed, paraffin-embedded tissue sections cut at a thickness of 5 μm on positively charged microscope slides. Paraffin was removed from the sections with three washes of 5 min each in CitriSolve. The slides were then hydrated in two washes of absolute ethanol for 1 min each and allowed to air dry. The slides were processed through a pretreatment solution of sodium thiocyanate, which had been preheated to 80 °C. After a 3-min wash in distilled water, the tissue was digested in protease solution (pepsin in 0.2 N HCl; Vysis protease, Abbott Molecular, 02J02-032) for 15 min at 37 °C, followed by another 3-min wash in distilled water. The slides were allowed to air dry and were then dehydrated by passing them through consecutive 70%, 85% and 100% ethanol solutions for 1 min each. The slides were again allowed to air dry before applying the prepared probe mixture. The probes used were to *TNFRSF1B* and a chromosome 1q11 control region (Empire Genomics). The probes were diluted in *t*DenHyb-2 hybridization buffer (Insitus Biotechnologies) and mixed well. Next, probe in buffer was applied to the appropriate slide to cover the tissue section, and the section was coverslipped. Co-denaturation was achieved by incubating the slides at 73 °C for 5 min in a slide moat. Hybridization occurred by transferring the slides to a 37 °C light-shielded, humidified slide moat overnight. After hybridization, coverslips were removed and the slides were immersed in 75 °C wash solution (2× SSC/0.3% NP-40) for 2 min followed by a 1-min wash in a jar containing the same solution at room temperature. The slides were allowed to air dry in the dark and were then counterstained with 10 μl of DAPI II (Abbott Molecular). Slides were examined using an Olympus BX60 fluorescent microscope with appropriate filters for Spectrum Orange, Spectrum Green and the DAPI counterstain.

cDNA synthesis and quantitative PCR.

cDNA was synthesized from total RNA (DNA free; Qiagen) using the iScript cDNA synthesis kit (Bio-Rad). Quantitative PCR was performed with Maxima SYBR Green qPCR master mix (Fermentas) on a LightCycler 480 instrument (Roche). Relative mRNA expression was calculated on the basis of normalization to *RPL32* levels (and additionally to *CD4* levels in the case of tumor samples).

Statistical analysis.

All experiments were performed in at least triplicate, and the statistics for various analyses are included in the relevant figure legends. Every effort was made to ensure that the statistical tests were appropriate for the assumed distributions of the sample sets. Variance was assumed to be approximately equal between sample groups when statistical testing was performed. GraphPad Prism was used to perform all *t* tests and survival curve analyses. Multivariate analysis was performed using the Cox proportional hazard model with Matlab 2014b, function coxphfit with censoring and a single-tailed *P* value.

Supplementary Material

Refer to Web version on PubMed Central for supplementary material.

ACKNOWLEDGMENTS

We thank A. Alizadeh, H. Chang, S. Artandi, L. Boxer, D. Webster and J. Kovalski for presubmission review of the manuscript. We thank all the patients who generously participated in this study. This work was supported by the Office of Research and Development of the US Department of Veterans Affairs and by US National Institutes of Health (NIH) grant R01CA142635 awarded to P.A.K. A.U. was supported by US NIH grant F32CA168091 and by the American Society of Hematology Research Training Award for Fellows. A.B. received support from US NIH grant F310CA180408. E.R. received support from the Dermatology Foundation. The studies were generously supported by the Haas Family Foundation and the Drs. Martin and Dorothy Spatz Charitable Foundation.

References

1. Wong HK , Mishra A , Hake T & Porcu P Evolving insights in the pathogenesis and therapy of cutaneous T-cell lymphoma (mycosis fungoides and Sezary syndrome). Br. J. Haematol 155, 150–166 (2011).21883142
2. Kiessling MK et al. High-throughput mutation profiling of CTCL samples reveals *KRAS* and *NRAS* mutations sensitizing tumors toward inhibition of the RAS/RAF/MEK signaling cascade. Blood 117, 2433–2440 (2011).21209378
3. Vaqué JP et al. *PLCG1* mutations in cutaneous T-cell lymphomas. Blood 123, 2034–2043 (2014). 24497536
4. So T & Croft M Regulation of PI-3-kinase and Akt signaling in T lymphocytes and other cells by TNFR family molecules. Front. Immunol 4, 139 (2013).23760533
5. Lee CS et al. Transcriptome sequencing in Sezary syndrome identifies Sezary cell and mycosis fungoides–associated IncRNAs and novel transcripts. Blood 120, 3288–3297 (2012).22936659
6. Newman AM et al. FACTERA: a practical method for the discovery of genomic rearrangements at breakpoint resolution. Bioinformatics 30, 3390–3393 (2014).25143292
7. Migliazza A et al. Heterogeneous chromosomal aberrations generate 3′ truncations of the *NFKB2/lyt-10* gene in lymphoid malignancies. Blood 84, 3850–3860 (1994).7949142
8. Zhang J , Chang CC , Lombardi L & Dalla-Favera R Rearranged *NFKB2* gene in the HUT78 T-lymphoma cell line codes for a constitutively nuclear factor lacking transcriptional repressor functions. Oncogene 9, 1931–1937 (1994).8208540
9. Vasmatzis G et al. Genome-wide analysis reveals recurrent structural abnormalities of *TP63* and other p53-related genes in peripheral T-cell lymphomas. Blood 120, 2280–2289 (2012).22855598
10. Nguyen LT & Ohashi PS Clinical blockade of PD1 and LAG3—potential mechanisms of action. Nat. Rev. Immunol 15, 45–56 (2015).25534622
11. Ashkenazi A & Dixit VM Death receptors: signaling and modulation. Science 281, 1305–1308 (1998).9721089
12. Shin JH et al. Positive conversion of negative signaling of CTLA4 potentiates antitumor efficacy of adoptive T-cell therapy in murine tumor models. Blood 119, 5678–5687 (2012).22538857
13. Mellman I , Coukos G & Dranoff G Cancer immunotherapy comes of age. Nature 480, 480–489 (2011).22193102
14. Sekulic A et al. Personalized treatment of Sezary syndrome by targeting a novel *CTLA4:CD28* fusion. Mol. Genet. Genomic Med 3, 130–136 (2015).25802883
15. Cabal-Hierro L & Lazo PS Signal transduction by tumor necrosis factor receptors. Cell. Signal 24, 1297–1305 (2012).22374304
16. van Doom R et al. Oncogenomic analysis of mycosis fungoides reveals major differences with Sezary syndrome. Blood 113, 127–136 (2009).18832135
17. Heemann C et al. Circulating levels of TNF receptor II are prognostic for patients with peripheral T-cell non-Hodgkin lymphoma. Clin. Cancer Res 18, 3637–3647 (2012).22573350
18. Lin WM et al. Characterization of the DNA copy-number genome in the blood of cutaneous T-cell lymphoma patients. J. Invest. Dermatol 132, 188–197 (2012).21881587
19. Rodríguez M et al. NF-κB signal triggering and termination by tumor necrosis factor receptor 2. J. Biol. Chem 286, 22814–22824 (2011).21558270

20. Zinzani PL et al. Phase II trial of proteasome inhibitor bortezomib in patients with relapsed or refractory cutaneous T-cell lymphoma. J. Clin. Oncol 25, 4293–4297 (2007).17709797
21. Acuto O & Michel F CD28-mediated co-stimulation: a quantitative support for TCR signalling. Nat. Rev. Immunol 3, 939–951 (2003)14647476
22. Li H & Durbin R Fast and accurate long-read alignment with Burrows-Wheeler transform. Bioinformatics 26, 589–595 (2010).20080505
23. DePristo MA et ai. A framework for variation discovery and genotyping using next-generation DNA sequencing data. Nat. Genet 43, 491–498 (2011).21478889
24. Koboidt DC et ai. VarScan: variant detection in massively parallel sequencing of individual and pooled samples. Bioinformatics 25, 2283–2285 (2009).19542151
25. Deng X SeqGene: a comprehensive software solution for mining exome- and transcriptome-sequencing data. BMC Bioinformatics 12, 267 (2011).21714929
26. Ng SB et al. Targeted capture and massively parallel sequencing of 12 human exomes. Nature 461, 272–276 (2009).19684571
27. Liu X , Jian X & Boerwinkie E dbNSFP v2.0: a database of human non-synonymous SNVs and their functional predictions and annotations. Hum. Mutat 34, E2393–E2402 (2013).23843252
28. Kim D et al. TopHat2: accurate alignment of transcriptomes in the presence of insertions, deletions and gene fusions. Genome Biol 14, R36 (2013).23618408
29. Shi J & Walker MG Gene set enrichment analysis (GSEA) for interpreting gene expression profiles. Curr. Bioinformatics 2, 133–137 (2007).
30. Cong L et al. Multiplex genome engineering using CRISPR/Cas systems. Science 339, 819–823 (2013).23287718

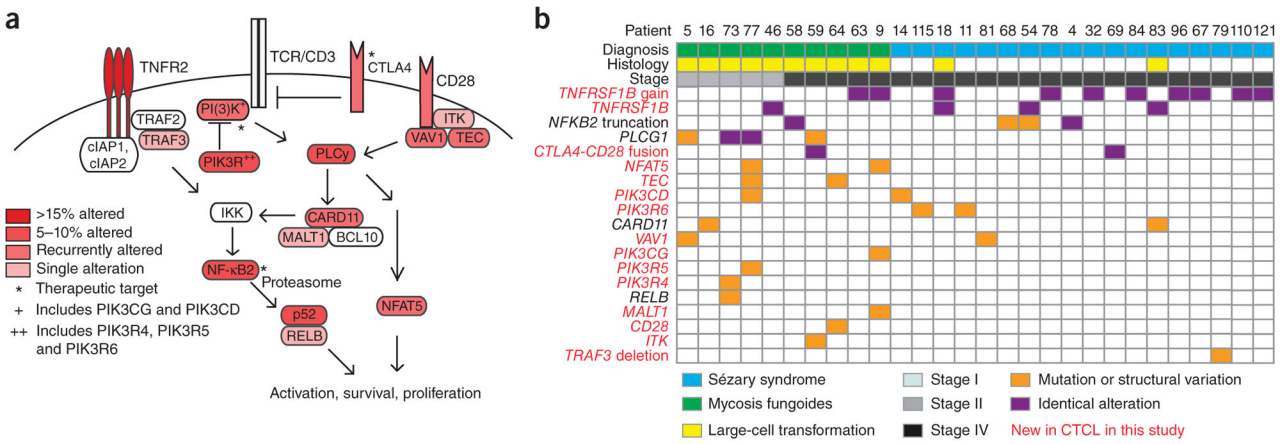

Figure 1.

Recurrent alterations in T cell survival and activation pathways in mycosis fungoides and Sézary syndrome. (**a**) Pathway diagram of interacting T cell survival and activation pathways. The incidence of alterations, including mutations and genomic structural variations, in 73 resequenced pairs of mycosis fungoides or Sézary syndrome samples and matched normal samples is indicated by the shade of red. Asterisks indicate drug targets, and plus signs indicate the inclusion of multiple family members. (**b**) Characterization of pairs of mycosis fungoides or Sézary syndrome samples and matched normal samples in the pathway represented in **a**. Recurrent identical amino acid alterations are indicated by purple shading.

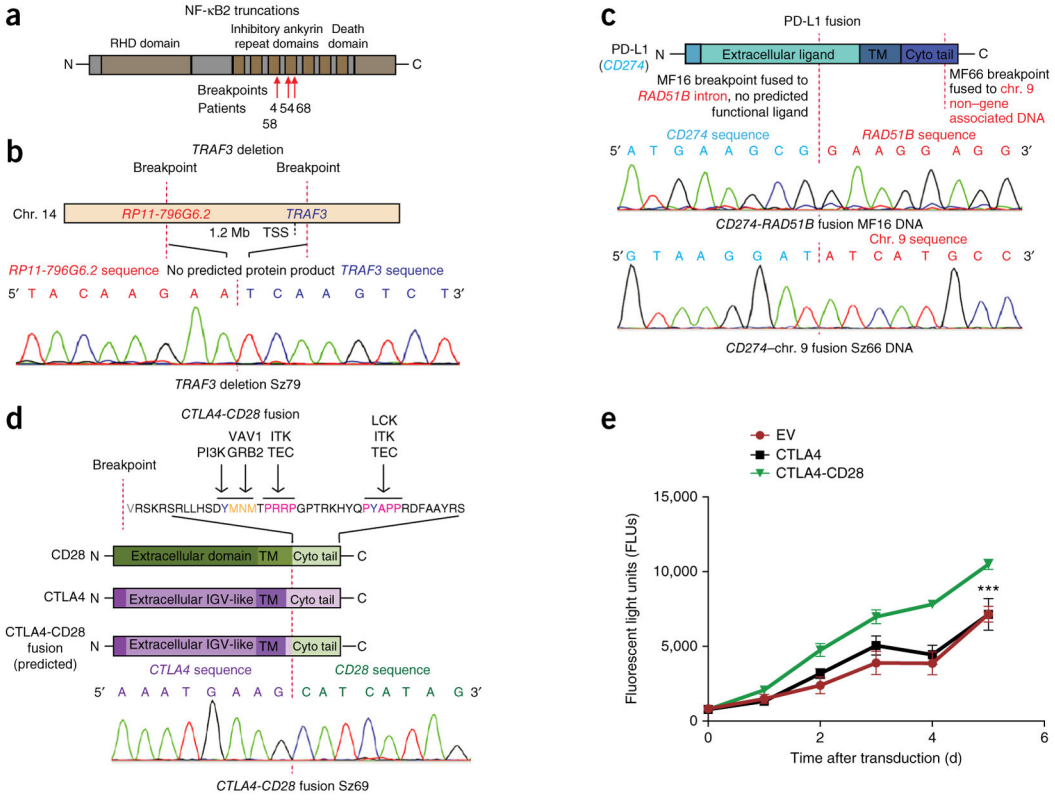

Figure 2.

Mycosis fungoides and Sézary syndrome are characterized by recurrent structural variations. (**a**) Diagram of the NF-κB2 p100 protein with red arrows denoting breakpoint locations. The numbers below represent patients with mycosis fungoides (MF) and Sézary syndrome (Sz). RHD, Rel homology domain. (**b**) Diagram representing the genomic deletion on chromosome 14 removing 1.2 Mb of sequence, including the transcription start site (TSS) and 5′ portion of *TRAF3*, resulting in no predicted TRAF3 protein product. The genomic breakpoints of the chromosome 14 deletion were validated by Sanger sequencing in Sézary syndrome 79. (**c**) Diagram showing the PD-L1 (*CD274*) breakpoints in Sézary syndrome 66 and mycosis fungoides 16. Sanger sequencing was used to validate the genomic breakpoints in *CD274* in these patients. TM, transmembrane domain; cyto tail, cytoplasmic tail. (**d**) Diagram of the *CTLA4-CD28* fusion including the breakpoints and fusion product. The CD28 cytoplasmic tail has several known binding sites for signaling partners, as indicated. Blue tyrosine residues include known phosphorylation sites. TM, transmembrane region; cyto tail, cytoplasmic tail[21]. The genomic breakpoints of the *CTLA4-CD28* fusions were validated by Sanger sequencing; the chromatogram is shown for Sézary syndrome 69. (**e**) Jurkat cell proliferation as measured by a fluorescent viability assay in cells transduced with empty vector (EV) or those expressing CTLA4 or the CTLA4-CD28 fusion construct; $n = 3$ biological replicates. Data are shown as means ± s.e.m. *** $P<0.0001$.

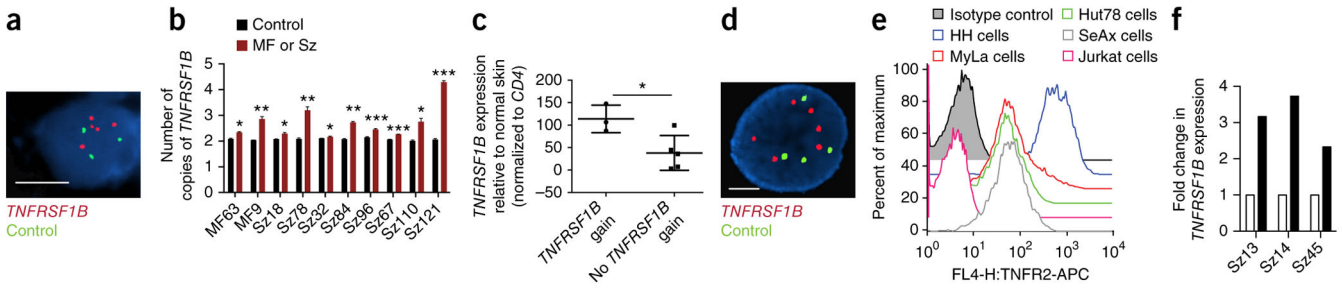

Figure 3.

Genomic gains affect the expression of TNFR2. (**a**) Image of FISH analysis for *TNFRSF1B* (red) and a control region (green) in a cell with *TNFRSF1B* (TNFR2) gain. Scale bar, 10 microns. (**b**) Graph indicating the number of copies of *TNFRSF1B* that were present in each control sample or mycosis fungoides or Sézary syndrome sample. Means ± s.d. are shown. $*P < 0.05$, $**P < 0.01$, $***P < 0.001$, two-tailed *t* test. (**c**) Plot of *TNFRSF1B* transcript levels in stage IV mycosis fungoides tumors with *TNFRSF1B* gain ($n = 3$) in comparison to tumors without gain ($n = 5$). Bars show the range of expression, with points showing exact values for each of the eight samples tested. Transcript levels were determined by quantitative PCR and normalized to *CD4* transcript levels; relative expression is shown in comparison to that for normal human skin. $*P < 0.05$, two-tailed *t* test. (**d**) Image of FISH analysis for *TNFRSF1B* (red) and a control region (green) in an HH cell, validating copy gain in this cell line. Scale bar, 10 microns. (**e**) CTCL cell lines stained with antibody to TNFR2 or isotype control and analyzed using flow cytometry. (**f**) *TNFRSF1B* is overexpressed at the mRNA level in all three Sézary syndrome samples (black bars) relative to matched normal control samples in published data (white bars)[5].

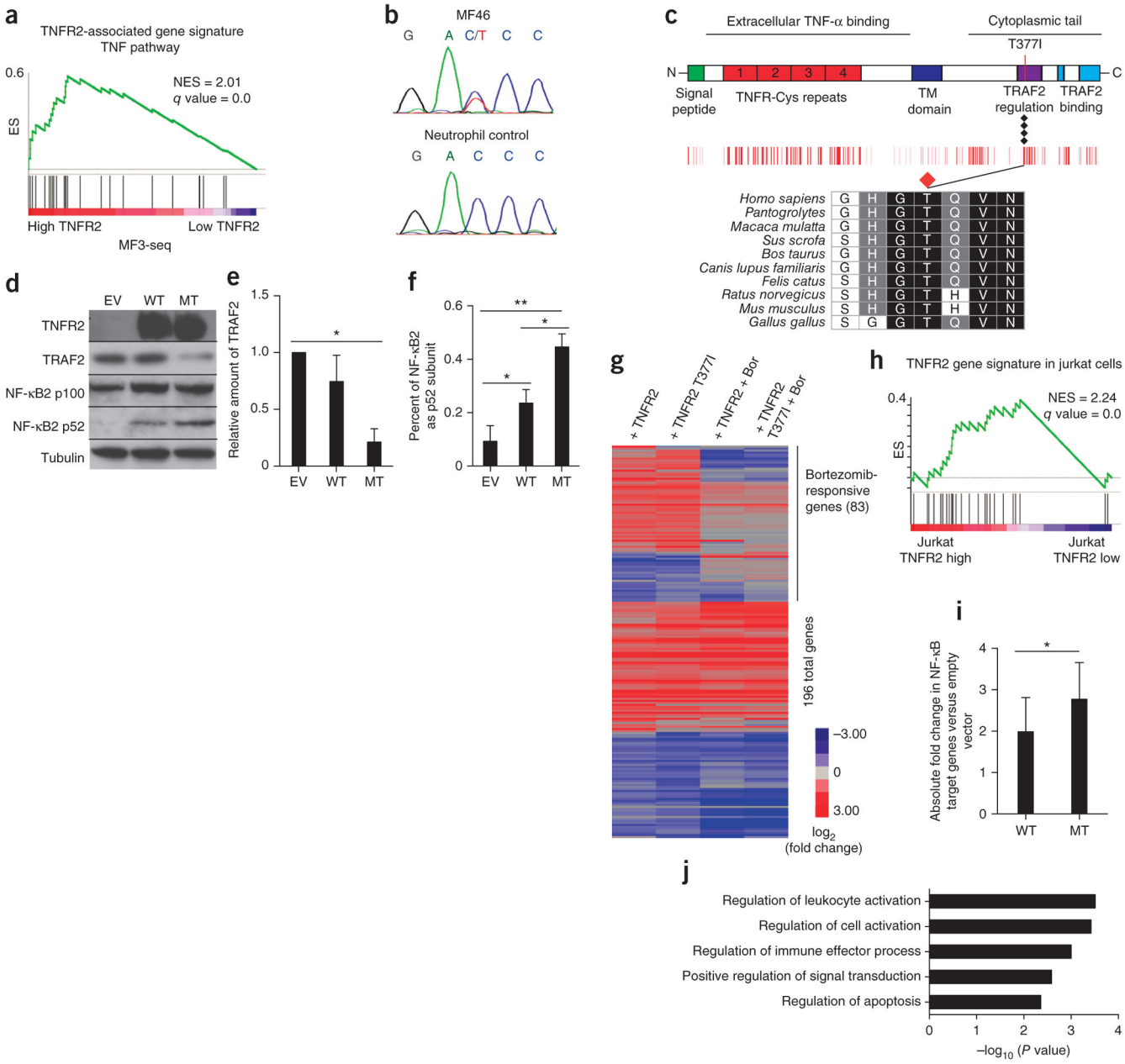

Figure 4.

TNFR2 p.Thr377Ile alterations activate non-canonical NF-κB2 signaling. (**a**) TNFR2 expression levels in mycosis fungoides 3-seq data[5] are highly correlated with a TNF pathway gene signature (Molecular Signatures Database). The GSEA enrichment plot is shown. NES, normalized enrichment score; ES, enrichment score. (**b**) The TNFR2 p.Thr377Ile alteration was confirmed by Sanger sequencing in mycosis fungoides 46 relative to a control. (**c**) Diagram of the TNFR2 protein indicating the location of the altered residue in the TRAF2 regulation domain. The conservation scores below were derived from dbNSFP and are shown in red in the heat map (red is the degree of conservation as measured by the dbSNP composite score, with the highest score 5 being the most intense red). (**d**)

Immunoblots of Jurkat cells transduced with empty vector or vector encoding wild-type TNFR2 (WT) or TNFR2 Thr377Ile (MT); the whole blots are shown in Supplementary Figure 8. (**e**) Quantification of TRAF2 levels relative to those in cells transduced with empty vector; data are shown as means ± s.e.m. ($n = 3$). *$P < 0.05$. (**f**) Quantification of NF-κB2 p52 levels as a percentage of total NF-κB2 protein levels; data are shown as means ± s.e.m. ($n = 3$). *$P < 0.05$, **$P < 0.001$. (**g**) Heat map showing $\log_2$ (fold change) in the levels of transcripts changing by ≥2-fold in RNA sequencing in Jurkat cells expressing either wild-type or mutant TNFR2 as compared with cells transduced with empty vector or in the same cells treated with 10 μM bortezomib (Bor) for 6 h. (**h**) GSEA enrichment plot of Jurkat cells expressing TNFR2 showing significant enrichment for the TNFR2 TNF pathway signature identified in **a**. (**i**) Average fold change in the levels of NF-κB target transcripts for cells expressing wild-type or mutant TNFR2; data are shown as means ± s.d. ($n = 15$ genes). *$P < 0.05$. (**j**) Gene Ontology (GO) enrichment terms of genes responsive to bortezomib treatment, as marked in **g**.